Los Alamos
NATIONAL LABORATORY
Research Note
Applied Physics Division
Group X-5, Diagnostic Applications

To/MS: Distribution
From/MS: David Ketcheson
Phone/FAX: (206)-616-8703
Symbol: X-5-RN(U)05-35 (LA-UR-05-7048)
Date: October 20, 2005

Inverse Solution Methods and Perturbation Estimates for Radiation Leakage without Scattering

Abstract

The inverse problem of estimating system parameters from measurements of radiation leakage from a decay gamma source surrounded by a series of concentric spherical shield layers is considered. It is assumed that measured lines are well resolved and that any scattered photons are removed from the line; therefore, scattering is ignored. With this approximation, the transport equation is solved semi-analytically using ray tracing. Gradients of the calculated leakage with respect to the parameters are evaluated either by adjoint differentiation or by differentiation of the ray trace expression for the leakage. These gradients are used in gradient-based root-finding and optimization methods. The resulting methods are able to estimate unknown source and shield thicknesses, densities, and compositions using only measured gamma-ray leakage fluxes. These methods using semi-analytic gradients are compared with existing methods using discrete ordinates calculations and adjoint differentiation. The ray trace derivatives are more accurate and computationally efficient, resulting in a faster and more robust inverse solution. Perturbation estimates for internal interface perturbations are considered, and estimates are developed that are highly accurate over a very large range of perturbations.

I Introduction A direct solution to the Boltzmann transport equation for a given system results in the particle angular flux for the system. However, the real problem is frequently the inverse: given the angular flux or some functional of it (e.g., the particle flux at a detector), what is the system?

Favorite developed a root-finding inverse method, based on inversion of a variational functional and using Newton-Raphson iteration [2]. Buescher & Vaughan developed a surrogate search method specially tailored to the problem of a spherical source surrounded by concentric sphere shield layers [1]. Favorite & Sanchez implemented a root-finding method using adjoint-based derivatives [5].

In this work, we consider improvements to both gradient-based search methods and direct search methods. For gradient methods, ray tracing is used to calculate more accurate gradients with greater computational efficiency. For direct methods, more accurate perturbation estimates are developed.

The rest of the paper is laid out as follows. In section II, we define the problem of interest and derive ray trace solutions for the leakage and forward and adjoint fluxes, taking into account the no-scattering approximation and 1D spherical geometry. We also present a method for calculating

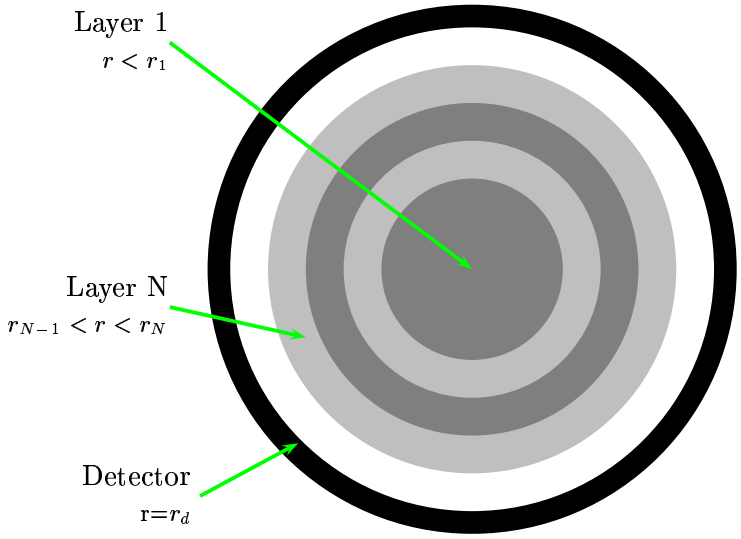

FIG. 1. *General problem setup*

derivatives of the leakage directly from the ray trace solution. In section III, we derive expressions for leakage derivatives using adjoint differentiation. In section IV, we derive and test highly accurate leakage estimates for internal interface perturbations. In section V, we present the details of two iterative algorithms to solve the inverse problem using the ray trace and adjoint derivatives. In section VI, the inverse methods are tested on a series of problems.

II Problem Definition and Ray Trace Solution Consider the transport of gamma rays of discrete energies in an arrangement of N concentric spherical shells, as depicted in figure 1. Layer n extends from inner radius r_{n-1} to outer radius r_n. Each layer is homogeneous, with macroscopic absorption cross section $\Sigma^g_{t,n}$ cm^{-1} and volumetric source rate q^g_n cm^{-3} s^{-1} for gamma rays of energy group g.

Gamma ray transport, in the absence of scattering, is governed by the Boltzmann transport equation:

$$\hat{\Omega} \cdot \nabla \psi + \Sigma_t \psi = q. \tag{1}$$

The quantity of interest in this work is the detector signal (leakage)

$$M = < \Sigma_d \psi >, \tag{2}$$

where Σ_d is the detector response function. The adjoint flux ψ^* satisfies

$$-\hat{\Omega} \cdot \nabla \psi^* + \Sigma_t \psi^* = \Sigma_d. \tag{3}$$

The inverse methods and perturbation estimates we will use require calculation of the forward and adjoint fluxes as functions of position and angle. The solution for the forward flux at points lying outside all source and shield layers has been worked out previously [7]. We now consider the general solution for points that may lie inside the source/shield system, as well as for the adjoint flux.

II.A Single, central source In this section we suppose, for simplicity, that only the central sphere emits radiation:

$$q_1^g = q^g \tag{4}$$
$$q_n^g = 0 \quad (n > 0). \tag{5}$$

II.A.i Forward Flux The angular flux at r, $r_{n-1} < r < r_n$ and angle $\theta - \pi$ can be found by tracing a ray from r in direction θ, yielding

$$\psi(r, \theta - \pi) = \frac{1}{2}\frac{q}{\Sigma_1} e^{-\left(\sum_{i=2}^{N} \Sigma_i D_{n,i}\right)} (1 - e^{-2\Sigma_1 D_{n,1}}), \tag{6}$$

where $D_{n,i}(r, \theta)$ is the length of the ray's path through layer i. The angle-integrated flux is

$$\psi(r) = 2\int_0^{arcsin(r_1/r)} sin(\theta)\psi(r, \theta - \pi)d\theta \tag{7}$$
$$= \frac{q}{\Sigma_1}\int_0^{arcsin(r_1/r)} sin(\theta) e^{-\left(\sum_{i=2}^{N} \Sigma_i D_{n,i}\right)} (1 - e^{-2\Sigma_1 D_{n,1}})d\theta. \tag{8}$$

II.A.ii Leakage The angular flux at the detector radius, r_d, outside all source and shield layers is

$$\psi(r_d, \theta) = \frac{1}{2}\frac{q}{\Sigma_1} e^{-\left(\sum_{n=2}^{N} \Sigma_n (d_n - d_{n-1})\right)} (1 - e^{-2\Sigma_1 d_1}), \tag{9}$$

where

$$d_n = \sqrt{r_n^2 - r_d^2 sin^2(\theta)}. \tag{10}$$

We define the detector response to be

$$\Sigma_d = cos(\theta_d)\delta(r - r_d), \tag{11}$$

where θ_d denotes the angle of the particle's path at $r = r_d$.

The leakage is given by

$$M = \int_\theta \int_V \psi(r, \theta) sin(\theta) cos(\theta) \delta(r - r_d) dV d\theta \tag{12}$$
$$= 4\pi r_d^2 \int_\theta \psi(r_d, \theta) sin(\theta) cos(\theta) d\theta \tag{13}$$
$$= 2\pi r_d^2 \frac{q}{\Sigma_1}\int_0^{arcsin(r_1/r_d)} sin(\theta) cos(\theta) e^{-\left(\sum_{n=2}^{N} \Sigma_n (d_n - d_{n-1})\right)} (1 - e^{-2\Sigma_1 d_1}) d\theta. \tag{14}$$

It is convenient to make the change of variables $u = -cos(\theta)$, yielding

$$M = 2\pi r_d^2 \frac{q}{\Sigma_1}\int_{-1}^{-\sqrt{1-(r_1/r_d)^2}} -u e^{-\left(\sum_{n=2}^{N} \Sigma_n (d_n - d_{n-1})\right)} (1 - e^{-2\Sigma_1 d_1}) du \tag{15}$$

where

$$d_n = \sqrt{r_n^2 - r_d^2(1 - u^2)}. \tag{16}$$

II.A.iii Adjoint Flux We make the simplifying assumption that the detector distance is $r_d = \infty$. The adjoint source integrated over any ray is then simply unity. The adjoint flux at r, $r_{n-1} < r < r_n$ can then be written as

$$\psi^*(r,\theta) = \frac{1}{2} e^{-\left(\sum_{i=1}^{N} \Sigma_i D_{n,i}\right)}, \tag{17}$$

where $D_{n,i}$ is the length of the ray's path through layer i. The angle-integrated adjoint flux is

$$\begin{aligned} \psi^*(r) &= 2\int_0^{\pi} sin(\theta)\psi^*(r,\theta)d\theta & (18)\\ &= \int_0^{\pi} sin(\theta) e^{-\left(\sum_{i=1}^{N} \Sigma_i D_{n,i}\right)} d\theta. & (19) \end{aligned}$$

II.B Leakage Derivatives In order to solve the inverse problem using gradient-based search methods, we need a way to calculate the derivative of the leakage with respect to the unknown parameters. Highly accurate values may be obtained by differentiating the ray-trace leakage analytically and evaluating the resulting integrals numerically.

II.B.i Unknown Radii For inverse problems with unknown material radii, we will need to evaluate the partial derivatives of the solution with respect to the r_n. For $n > 1$ (i.e., non-source interfaces),

$$\frac{\partial M_d^g}{\partial r_n} = 4\pi r_d^2 \Delta\Sigma_{t,n} \int_{-1}^{-\sqrt{1-(r_1/r_d)^2}} -u\psi(r_d,u) \frac{r_n}{\sqrt{r_n^2 - r_d^2(1-u^2)}} du \tag{20}$$

where

$$\Delta\Sigma_{t,n} = \Sigma_{t,n+1} - \Sigma_{t,n}. \tag{21}$$

To find the derivative with respect to the source radius, we use the identity

$$\frac{\partial}{\partial x}\int_{y_0}^{f(x)} g(x,y)dy = g(x,f(x))\frac{df}{dx} + \int_{y_0}^{f(x)} \frac{\partial g}{\partial x} dy. \tag{22}$$

It is easy to show that the first term vanishes in our case. Thus

$$\frac{\partial M}{\partial r_1} = 2\pi r_d^2 \frac{q}{\Sigma_{t,1}} \int_{-1}^{-\sqrt{1-(r_1/r_d)^2}} \frac{-r_1 u}{\sqrt{r_1^2 - r_d^2(1-u^2)}} e^{-\left(\sum_{n=2}^{N} \Sigma_{t,n}(d_n - d_{n-1})\right)} \left(\Sigma_{t,2} + (2\Sigma_{t,1} - \Sigma_{t,2}) e^{-2\Sigma_{t,1} d_1}\right) du \tag{23}$$

II.B.ii Known Thicknesses, Unknown Locations Consider an inverse problem where the thickness of some material, e.g. a shield layer, is known, but the location of the layer is not. The leakage can be written in terms of the various thicknesses using

$$r_n = \sum_{i=1}^{n} T_n. \tag{24}$$

This also yields an expression for the partial derivative of M with respect to T_n:

$$\frac{dM}{dT_n} = \sum_{i=1}^{N} \frac{\partial M}{\partial r_i} \frac{dr_i}{dT_n} = \sum_{i=n}^{N} \frac{\partial M}{\partial r_i}. \tag{25}$$

The necessary derivatives have already been calculated above.

II.B.iii Unknown Source Weight Fractions Next we derive an expression for the derivative of the leakage with respect to the source component weight fractions. The chain rule yields

$$\frac{\partial M}{\partial f} = \frac{\partial M}{\partial \Sigma_t} \frac{\partial \Sigma_t}{\partial f} + \frac{\partial M}{\partial q} \frac{\partial q}{\partial f}, \tag{26}$$

where f is the weight fraction. Since $M \propto q$ and $q \propto f$, we have

$$\frac{\partial M}{\partial q} \frac{\partial q}{\partial f} = M/f. \tag{27}$$

Similarly,

$$\frac{\partial \Sigma_t}{\partial f} = \frac{N_j \sigma_j}{f_j}. \tag{28}$$

Differentiating Equation (15) gives

$$\frac{\partial M}{\partial \Sigma_{t,1}} = 2\pi r_d^2 \frac{q}{\Sigma_{t,1}} \int_{-1}^{-\sqrt{1-(r_1/r_d)^2}} -u e^{-\left(\sum_{n=2}^{N} \Sigma_{t,n}(d_n - d_{n-1})\right)} \left(2d_1 e^{-2\Sigma_{t,1} d_1} - \frac{1 - e^{-2\Sigma_{t,1} d_1}}{\Sigma_{t,1}} \right) du \tag{29}$$

so that

$$\frac{\partial M}{\partial f} = \frac{N_j \sigma_j}{f_j} \frac{\partial M}{\partial \Sigma_t} + \frac{M}{f}, \tag{30}$$

with $\frac{\partial M}{\partial \Sigma_t}$ given by Eq. (29).

II.B.iv Unknown Material Densities Next we derive an expression for the derivative of the leakage with respect to the material density of layer n. The chain rule yields

$$\frac{\partial M}{\partial \rho_n} = \frac{\partial M}{\partial \Sigma_{t,n}} \frac{\partial \Sigma_{t,n}}{\partial \rho_n} + \frac{\partial M}{\partial q_n} \frac{\partial q_n}{\partial \rho_n}, \tag{31}$$

where ρ_n is the density of layer n. Since, for a single central source, $M \propto q_1$ and $q_1 \propto \rho_1$, we have

$$\frac{\partial M}{\partial q_n} \frac{\partial q_n}{\partial \rho_n} = M/\rho_n \delta_{n1}. \tag{32}$$

Similarly,

$$\frac{\partial \Sigma_{t,n}}{\partial \rho_n} = \frac{\Sigma_{t,n}}{\rho_n}. \tag{33}$$

For $n = 1$, $\frac{\partial M}{\partial \Sigma_{t,1}}$ is given by Eq. (29). For $n > 1$, differentiating Equation (15) gives

$$\frac{\partial M}{\partial \Sigma_{t,1}} = 2\pi r_d^2 \frac{q}{\Sigma_{t,1}} \int_{-1}^{-\sqrt{1-(r_1/r_d)^2}} -u(d_n - d_{n-1}) e^{-\left(\sum_{n=2}^{N} \Sigma_{t,n}(d_n - d_{n-1})\right)} \left(1 - e^{-2\Sigma_{t,1} d_1} \right) du \tag{34}$$

so that

$$\frac{\partial M}{\partial \rho_n} = \frac{\Sigma_{t,n}}{\rho_n} \frac{\partial M}{\partial \Sigma_t} + \frac{M}{\rho_n}, \tag{35}$$

with $\frac{\partial M}{\partial \Sigma_{t,n}}$ given by Eqs. (29,34).

II.C Generalization We again consider the problem of the previous section, but now allow the outer spheres to be sources.

II.C.i Forward Flux The angular flux at r, $r_{n-1} < r < r_n$ and angle $\theta - \pi$ can be found again by tracing along ray from r in direction θ, yielding

$$\psi(r, \theta - \pi) = \frac{1}{2} \sum_j \frac{q_j}{\Sigma_j} e^{-\left(\sum_{i \neq j}^{N} \Sigma_i D_{n,i,j}\right)} (1 - e^{-2\Sigma_j D_{n,j}}), \tag{36}$$

where $D_{n,i,j}(r, \theta)$ is the length of the ray's path through layer i, in the interval between source region j and r. The angle-integrated flux is

$$\begin{aligned} \psi(r) &= 2 \int_0^{arcsin(r_N/r)} sin(\theta) \psi(r, \theta - \pi) d\theta & (37) \\ &= \sum_j \frac{q_j}{\Sigma_j} \int_0^{arcsin(r_N/r)} e^{-\left(\sum_{i \neq j}^{N} \Sigma_i D_{n,i,j}\right)} (1 - e^{-2\Sigma_j D_{n,j}}) d\theta. & (38) \end{aligned}$$

II.C.ii Adjoint Flux The adjoint flux in the general case is again given by Eqn. (19).

II.C.iii Leakage The total leakage is given by

$$\begin{aligned} M &= \int_\theta \int_V \psi(r, \theta) sin(\theta) cos(\theta) \delta(r - r_d) dV d\theta & (39) \\ &= 4\pi r_d^2 \int_\theta \psi(r_d, \theta) sin(\theta) cos(\theta) d\theta & (40) \\ &= 2\pi r_d^2 \sum_j \frac{q_j}{\Sigma_j} \int_0^{arcsin(r_N/r_d)} sin(\theta) cos(\theta) e^{-\left(\sum_{i \neq j}^{N} \Sigma_i D_{n,i,j}\right)} (1 - e^{-2\Sigma_j D_{n,j}}) d\theta. & (41) \end{aligned}$$

Consider a photon emitted at radius r and angle Ω, where $r_{n-1} < r < r_n$. The length of the photon's path through sphere m is

$$D_{nm} = \begin{cases} 2\sqrt{r_m^2 - r^2 sin^2(\Omega)} \cdot H\left(r_m - r sin(\Omega)\right) & (m < n) \\ \sqrt{r_m^2 - r^2 sin^2(\Omega)} - \sqrt{r_{m-1}^2 - r^2 sin^2(\Omega)} & (m > n) \\ \sqrt{r_n^2 - r^2 sin^2(\Omega)} - r cos(\Omega) - 2\sqrt{r_{n-1}^2 - r^2 sin^2(\Omega)} \cdot H\left(r_{n-1} - r sin(\Omega)\right) & (m = n) \end{cases}, \tag{42}$$

where H is the Heaviside function and $r_0 = 0$.

We again make the change of coordinates $u = -cos(\Omega)$, yielding

$$D_{nm} = \begin{cases} 2\sqrt{r_m^2 - r^2(1 - u^2)} \cdot H\left(u^2 - (1 - r_m^2/r^2)\right) & (m < n) \\ \sqrt{r_m^2 - r^2(1 - u^2)} - \sqrt{r_{m-1}^2 - r^2(1 - u^2)} & (m > n) \\ \sqrt{r_n^2 - r^2(1 - u^2)} + ru - 2\sqrt{r_{n-1}^2 - r^2(1 - u^2)} \cdot H\left(u^2 - (1 - r_{n-1}^2/r^2)\right) & (m = n) \end{cases} \tag{43}$$

II.C.iv Generalized Leakage Derivatives It is possible to differentiate the general leakage (41) and use these partial derivatives in the inverse solution. However, the resulting expressions are extremely cumbersome. It is much simpler to use the ray trace forward and adjoint fluxes [Eqns. (38) and (19)] in the adjoint derivative formulas of the next section. For this reason, we will not pursue differentiation of (41).

III Adjoint Differentiation Previously developed inverse solution methods for this problem have employed adjoint differentiation [2, 3, 5] and discrete ordinates fluxes. In this section we present a unified formulation of these methods and discuss numerical issues related to their implementation.

We first find a general expression for the partial derivative $\frac{\partial M}{\partial x_n}$ using the adjoint solution. The derivation is similar to those of [3, 4].

Differentiating $M =< \Sigma_d \psi >$ gives

$$\frac{\partial M}{\partial x_n} =< \Sigma_d \frac{\partial \psi}{\partial x_n} > . \tag{44}$$

Differentiating the transport equation yields

$$L\frac{\partial \psi}{\partial x_n} = \frac{\partial q}{\partial x_n} - \frac{\partial \Sigma}{\partial x_n}\psi. \tag{45}$$

Substitution of (3) in (44) gives

$$\frac{\partial M}{\partial x_n} =< L^*\psi^* \frac{\partial \psi}{\partial x_n} >=< \psi^* L\frac{\partial \psi}{\partial x_n} > . \tag{46}$$

Now using (45), we have

$$\frac{\partial M}{\partial x_n} = < \psi^* \left(\frac{\partial q}{\partial x_n} - \frac{\partial \Sigma}{\partial x_n}\psi \right) > . \tag{47}$$

III..v Unknown Radii For the case $x_n = r_n$, we have

$$\frac{\partial q}{\partial x_n} = \frac{\partial q}{\partial r_n} = \Delta q_n \delta(r - r_n), \tag{48}$$

$$\frac{\partial \Sigma}{\partial x_n} = \frac{\partial \Sigma}{\partial r_n} = \Delta \Sigma_n \delta(r - r_n), \tag{49}$$

where

$$\Delta q_n = q_n - q_{n+1} \tag{50}$$

$$\Delta \Sigma_n = \Sigma_n - \Sigma_{n+1}. \tag{51}$$

Now using (47), we have

$$\frac{\partial M}{\partial r_n} = < \psi^* \left(\Delta q_n - \Delta \Sigma_n \psi\right) \delta(r - r_n) > \tag{52}$$

$$\frac{\partial M}{\partial r_n} = 4\pi r_n^2 \psi^*(r_n) \left(\Delta q_n - \Delta \Sigma_n \psi(r_n)\right) . \tag{53}$$

III..vi Unknown Thicknesses As with the ray trace derivatives, we can use Equation (25) with the derivatives just found above to calculate derivatives of M with respect to unknown thicknesses.

III..vii Unknown Source Weight Fractions For the case $x_n = f_i$, we have

$$\frac{\partial q}{\partial x_n} = \frac{\partial q}{\partial f_i} = q\frac{\rho_s N_A}{A_i}, \tag{54}$$

$$\frac{\partial \Sigma}{\partial x_n} = \frac{\partial \Sigma}{\partial f_i} = \rho_s N_A \sum_{j=1}^{J} \frac{\sigma_{t,j}}{A_j}. \tag{55}$$

So

$$\frac{\partial M}{\partial f_i} = \rho_s N_A < \psi^* \left(\frac{q}{A_i} - \sum_{j=1}^{J} \frac{\sigma_{t,j}}{A_j}\psi \right) > . \tag{56}$$

III..viii Unknown Material Densities For the case $x_n = \rho_n$, noting that q and Σ_t are both linear functions of ρ, we have

$$\frac{\partial q}{\partial x_n} = \frac{\partial q}{\partial \rho_n} = \frac{q_n}{\rho_n} H_p \tag{57}$$

$$\frac{\partial \Sigma_t}{\partial x_n} = \frac{\partial \Sigma_t}{\partial \rho_n} = \frac{\Sigma_{t,n}}{\rho_n} H_p, \tag{58}$$

where

$$H_p(r) = \begin{cases} 1 & r \in V_p \\ 0 & r \notin V_p \end{cases} \tag{59}$$

Substituting (57-58) into (47), we have

$$\frac{\partial M}{\partial \rho_n} = \frac{1}{\rho_n} \left(< \psi^* q_n >_p - < \psi^* \Sigma_n \psi >_p \right), \tag{60}$$

where $< \cdot >_p$ denotes an inner product over only V_p. For density perturbations of source materials, the difference between the two terms in (60) is much smaller than either term, so small errors in the fluxes often lead to derivatives with not even one digit of accuracy. In such cases, it may be useful to rewrite the derivative as

$$\frac{\partial M}{\partial \rho_n} = \frac{1}{\rho_n} < \psi^* \left(q_n - \Sigma_n \psi \right) >_p, \tag{61}$$

$$= \frac{1}{\rho_n} < \psi^* \left(L - \Sigma_n \right) \psi >_p, \tag{62}$$

$$= \frac{1}{\rho_n} < \psi^* \left(\hat{\Omega} \cdot \nabla \psi \right) >_p . \tag{63}$$

IV Perturbation Estimates In this section, we consider the following problem: given the fluxes ψ, ψ^* and leakage M for a given (unperturbed) problem with absorption Σ_t and source q, estimate the leakage M' for the perturbed problem with absorption and source

$$\Sigma_t' = \Sigma_t + \Delta\Sigma_t \tag{64}$$
$$q' = q + \Delta q. \tag{65}$$

We first describe various methods of estimating M', and then compare results for several test cases.

The perturbed absorption and source are assumed to result from an internal interface perturbation. It is important to note the particular nature of such perturbations . Traditional perturbations have magnitude $\mathcal{O}(\epsilon)$ and support over a region of $\mathcal{O}(1)$. However, internal interface perturbations are of magnitude $\mathcal{O}(1)$ and extend over a region of $\mathcal{O}(\epsilon)$. Perturbations are traditionally written as

$$\Sigma_t' = \Sigma_t + \epsilon\Sigma_t^1 \tag{66}$$
$$q' = q + \epsilon q^1, \tag{67}$$

where $||\Sigma_t^1|| = \mathcal{O}(1)$. In the internal interface perturbation case, while $||\Sigma_t^1||_1 = \mathcal{O}(1)$, clearly $||\Sigma_t^1||_\infty = \mathcal{O}(1/\epsilon)$. Instead, we can write perturbations as

$$\Sigma_t'(x) = \Sigma_t(x - \epsilon X(x)) \tag{68}$$
$$q'(x) = q(x - \epsilon X(x)), \tag{69}$$

where

$$X(r) = \begin{cases} 1 & r \in V_p \\ 0 & r \notin V_p \end{cases} \tag{70}$$

We refer to Eqns. (68-69) as *coordinate perturbations*. Later we will see how coordinate perturbed approximations may lead to improved perturbed leakage estimates.

IV.A Taylor and Variational Estimates A second-order accurate approximation to M' can be obtained by taking just the first two terms in a Taylor series about the unperturbed value of x:

$$M' \approx M + (\nabla_x M)^T \Delta x = M + \sum_n \frac{\partial M}{\partial r_n} \Delta r_n \tag{71}$$

where $\Delta r = r' - r$ is the difference between the perturbed and unperturbed interface radii. The gradient $\nabla_x M$ may be obtained using Eqn. (47) with ray trace forward and adjoint fluxes.

Note that it is not possible to obtain higher-order approximations for perturbations of source interfaces by differentiating Eqn. (23) or Eqn. (53). The former fails because the integrand is singular; the latter, because Eqn. (52) involves a delta-function.

Second-order accurate approximations to M' may also be obtained from the Schwinger or Roussopolos variational principles. The variational estimates necessarily agree with the Taylor series approximations to first order; they differ only in the second- and higher-order (error) terms. The Roussopolos estimate can be reduced to [4]

$$M_R = M + < \psi^*(\Delta q - \psi\Delta\Sigma) >_p . \tag{72}$$

The Schwinger estimate can be reduced to [4]

$$M_S = M\frac{< \psi^* q > + < \psi^* \Delta q >_p}{< \psi^* q > + < \psi^* \Delta\Sigma\psi >_p}. \tag{73}$$

In [4], a new variational functional was introduced, combining the Roussopolos and Schwinger functionals. The combined functional can be reduced to [4]

$$M_C = M\frac{< \psi^* q > + < f\psi^* \Delta q >_p}{< \psi^* q > + < f\psi^* \Delta\Sigma\psi >_p} - < (1-f)\psi^*(\Delta\Sigma\psi - \Delta q) >_p . \tag{74}$$

Here, f is an arbitrary function that defines how to interpolate between the Roussopolos and Schwinger functionals.

The perturbed leakage is given exactly by

$$M' =< \Sigma_d \psi' > . \tag{75}$$

It can be shown that, if the perturbed adjoint flux $\psi^{*\prime}$ is used in place of ψ^* in either M_R or M_S, the exact perturbed leakage M' is obtained. Thus, the variational estimates may be made more accurate by using a trial function $\tilde{\psi}^*$ that more accurately approximates $\psi^{*\prime}$. In the next section, we consider methods for improving ψ^*.

IV.B Coordinate Perturbations Consider the monodirectional slab transport problem. Suppose that the location of all interfaces is shifted by distance ϵ: $r_n = r_n + \epsilon$. Then the perturbed flux ψ' satisfies

$$L(x-\epsilon)\psi' = q(x-\epsilon) \tag{76}$$

where $L(x)$ and $q(x)$ are the unperturbed transport operator and source. The perturbed flux can be obtained in terms of the unperturbed flux with a shift of coordinates:

$$\psi' = \psi(x-\epsilon). \tag{77}$$

Traditional perturbation theory would approximate ψ' using a series of the form

$$\tilde{\psi} = \psi + \epsilon\psi_1 + \epsilon^2\psi_2 + ... \tag{78}$$

where ψ_k are unknown functions of x. Comparing Eqn. (77) with Eqn. (78), the former is clearly advantageous because it is easily evaluated and exactly correct (with only a single term). The perturbed adjoint flux can be obtained from the unperturbed adjoint flux in the same manner.

Now consider the case where only r_2 is perturbed: $r_2 = r_2 + \epsilon$. From consideration of the exact solution, it can be seen that, in the perturbed interval (r_2, r_2'),

$$\psi^{*\prime}(x) = \psi^*(x-\epsilon) \tag{79}$$

as long as the magnitude of the perturbation is less than the thicknesses of the adjacent materials, i.e. $|\epsilon| <= min(r_3 - r_2, r_2 - r_1)$.

Now consider a general (single) interface perturbation, $r_n = r_n + \epsilon$. The adjoint flux in the perturbed region is given exactly by

$$\psi^{*\prime}(x) = \psi^*(x-\epsilon)e^{\Sigma_{t,n+1}\epsilon}. \tag{80}$$

We would like to apply Eq. (80) to interface perturbations in 1D spherical geometry as well. Eq. (80) can be applied directly to obtain estimates that are an improvement over the ordinary variational estimates; however, further improvement can be gained by assuming that for small perturbations,

$$\psi^{*\prime}(r) \approx \psi^*(r-\epsilon)e^{\gamma\Sigma_{t,n+1}\epsilon}. \tag{81}$$

in the perturbed region, where γ is a geometric factor that approximately accounts for the effect of rays passing obliquely through the perturbed region. In other words, γ is the average path length of a ray through the perturbed region, relative to the path length for rays that pass perpendicular to the perturbed interface. In the calculation of the inner product $< \psi^*\psi >$, the only rays that matter are those that pass through the source region, so we take the characteristic angle $\theta = \frac{1}{2}arcsin(r_1/r'_n)$ and use

$$\gamma = cos(\theta) = \sqrt{\frac{1}{2}(1+\sqrt{1-(r_1/r'_n)^2})}. \tag{82}$$

In the calculation of $< \psi^* >$, we set $\gamma = 1$.

In the numerical examples that follow, we apply coordinate perturbations to the reduced Roussopolos functional only. Improving the adjoint flux in the Schwinger and combined functionals would require finding an improved approximation outside the perturbed region.

IV.C Application to a Monodirectional Slab Problem We now test the coordinate perturbed Roussopolos estimate on the monodirectional slab problem used in [4].

The relative errors in perturbation estimates using the methods of the last section are plotted in Figure (2) for source perturbations of the monodirectional slab problem with a 0.3 cm slab source. The Taylor series approximations using ray trace and adjoint derivatives are both plotted, in order to verify that they are identical. The Roussopolos variational estimate is also identical to these two for this simple geometry. All three have a maximum error of about 27%. The coordinate-perturbed Roussopolos estimate, using Eq. (80) is a dramatic improvement. In fact it can be shown that for this simple problem, Eqn. (80) gives the exact perturbed adjoint flux in the perturbed region, so that the improved Roussopolos estimate is exact. In practice there is a very small error associated with evaluating the inner products by quadrature with a finite grid spacing.

IV.D Dimensional Analysis of Leakage From an Unshielded Sphere We now consider a different approach to finding approximate leakages and derivatives. Consider a spherical radiation source with no shielding. Let r_1 denote the source radius, and consider gamma rays of a single energy, with volumetric source rate q_n s^{-1} cm^{-3} and absorption coefficient Σ_t cm^{-1}.

The total leakage can be found by ray tracing to be (from Eq. (14))

$$M_d = 2\pi r_d^2 \frac{q}{\Sigma_t}\int_0^{arcsin(r_1/r_d)} sin(\theta)cos(\theta)(1-e^{-2\Sigma_t d(r_d,\theta)})d\theta. \tag{83}$$

The integral (83) cannot be evaluated analytically.

From physical principles, it is clear that the leakage must be independent of r_d, so long as $r_d \geq r_1$.

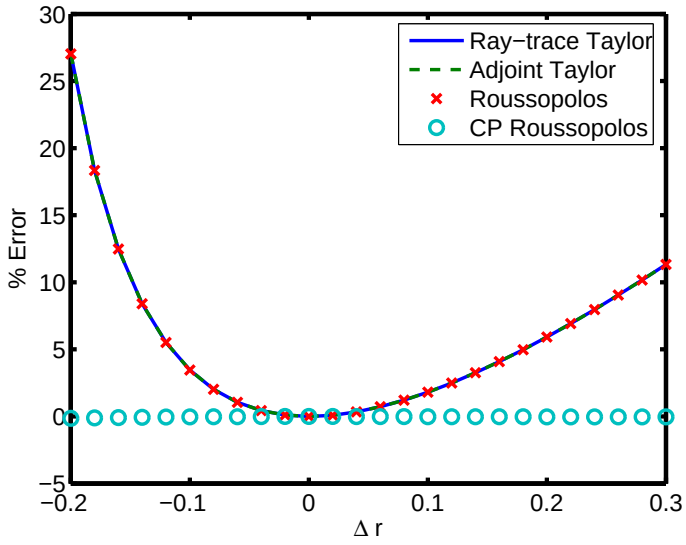

FIG. 2. *Perturbation estimate errors for 0.3 cm HEU slab source perturbations*

Thus, the leakage can only depend on q, Σ_t, and r_1, which have the following dimensions:

$$q = \frac{1}{L^3 T} \tag{84}$$

$$\Sigma_t = \frac{1}{L} \tag{85}$$

$$r_1 = L. \tag{86}$$

Here L is length and T is time. Since the leakage must be independent of the units used to measure length, we can eliminate r_1 and assume that

$$M_d = M_d(\bar{q}, \bar{\Sigma}_t), \tag{87}$$

where

$$\bar{q} = \frac{4}{3}\pi r_1^3 q \tag{88}$$

$$\bar{\Sigma}_t = \frac{4}{3}\Sigma_t r_1. \tag{89}$$

Clearly, $\bar{q}$ has the physical interpretation as the total source, integrated over the sphere, while $\bar{\Sigma}_t$ is proportional to the number of mean free paths in the sphere's diameter. Either physical reasoning or examination of (83) shows that M_d depends linearly on q, so we have that

$$M_d = \bar{q} g(\bar{\Sigma}_t), \tag{90}$$

where the function g is to be determined. Now, for $\bar{\Sigma}_t << 1$, most of the gammas emitted in the sphere will escape, so that $M_d \propto r_1^3$. On the other hand, For $\bar{\Sigma}_t >> 1$, only gammas emitted very

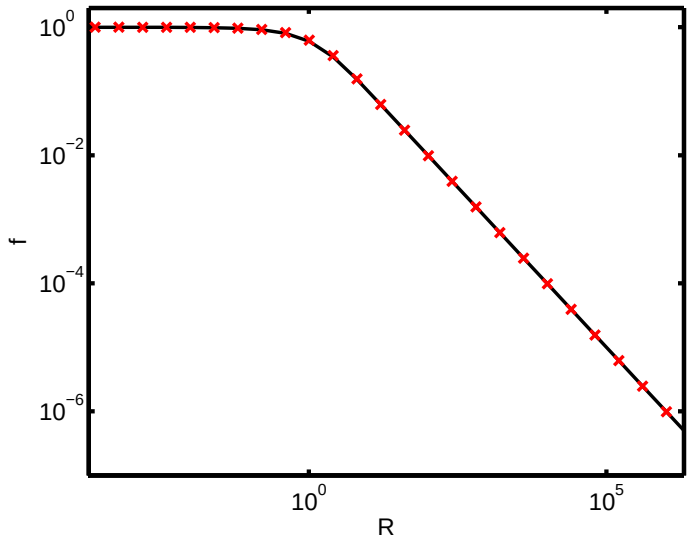

FIG. 3. *Empirical fit versus exact* $M_d/\bar{q}$

near the surface will escape, so that $M_d \propto r_1^2$. Thus

$$\lim_{\bar{\Sigma}_t \to 0} g = 1 \tag{91}$$

$$\lim_{\bar{\Sigma}_t \to \infty} g = \bar{\Sigma}_t^{-1}. \tag{92}$$

Notice that the coefficients in Eqs. (88-89) were chosen to simplify these limits, thereby simplifying the function g. A function that fits both these limits and also fits the function $M_d/\bar{q}$ quite well between them is

$$\tilde{g}(\bar{\Sigma}_t) = \frac{1 - e^{-\bar{\Sigma}_t}}{\bar{\Sigma}_t}. \tag{93}$$

In Figure 3, this function is plotted against the exact function $M_d/\bar{q}$. Note that substituting (93) in (90) yields

$$M_d \approx M_{SD} = \frac{\bar{q}}{\bar{\Sigma}_t}(1 - e^{-\bar{\Sigma}_t}) \tag{94}$$

which bears a striking resemblance to the monodirectional slab solution. Finally, using Eqs. (88-89), we have the *source depth* estimate

$$M_d \approx M_{SD} = \pi r_1^2 \frac{q}{\Sigma_t}(1 - e^{-\frac{4}{3}\Sigma_t r_1}) \tag{95}$$

It is possible to use Eq. (95) directly to obtain perturbed leakage estimates. However, a better estimate may be obtained using the exact unperturbed leakage and derivative. Examining Figure 3, it seems reasonable to suppose that

$$M_d(r_1) = \alpha(r_1) M_{SD}(r_1) \tag{96}$$

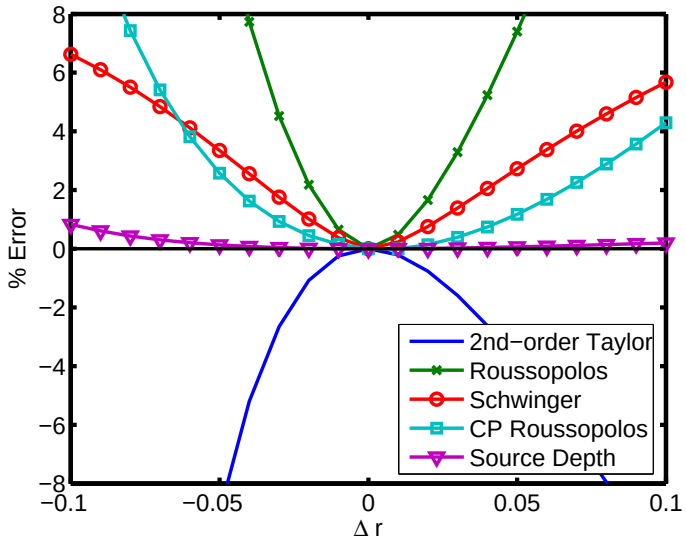

FIG. 4. *Perturbation estimate errors for 0.3 cm HEU spherical source perturbations with no shielding.*

where $\alpha(r_1) \approx 1$ is a slowly varying function of r_1. Then

$$\frac{dM_d}{dr_1} \approx \alpha(r_1)\frac{dM_{SD}}{dr_1} \tag{97}$$

since $\frac{d\alpha}{dr_1} \approx 0$.

Differentiating Eq. (95) gives an approximate value for the leakage derivative as a function of r_1. Given this, we can use the approximation

$$M(r_1') \approx M(r_1) + \alpha \int_{r_1}^{r_1'} \left.\frac{dM_{SD}}{dr_1}\right|_{r_1=\hat{r}_1} d\hat{r}_1 = M(r_1) + \left(\frac{dM}{dr_1}/\frac{dM_{SD}}{dr_1}\right)(M_{SD}(r_1') - M_{SD}(r_1)). \tag{98}$$

Eq. (98) is referred to as the SD estimate.

Figure 4 shows the perturbation estimate errors for perturbations of a 0.3 cm HEU source without shielding. The source depth estimate is clearly superior. Figure 5 shows errors for perturbations of the Godiva source without shielding. Although the Taylor, CP Roussopolos, and source depth estimates are all very accurate, the source depth estimate is significantly better than the other two. For the most severe perturbations shown, the source depth estimate error is smaller than the Taylor estimate error by three orders of magnitude.

Figures 6 and 7 show the errors for a -0.1 cm perturbation and a +0.1 cm perturbation (respectively) of an HEU source radius as a function of the unperturbed source radius. The source depth estimate is extremely accurate, even for the difficult case of small source radii.

IV.E The Exponential Estimate for Shield Interface Perturbations In [4], Favorite found that the combined variational functional, M_C, with $f = 1/\sqrt{2}$ gives an excellent estimate for

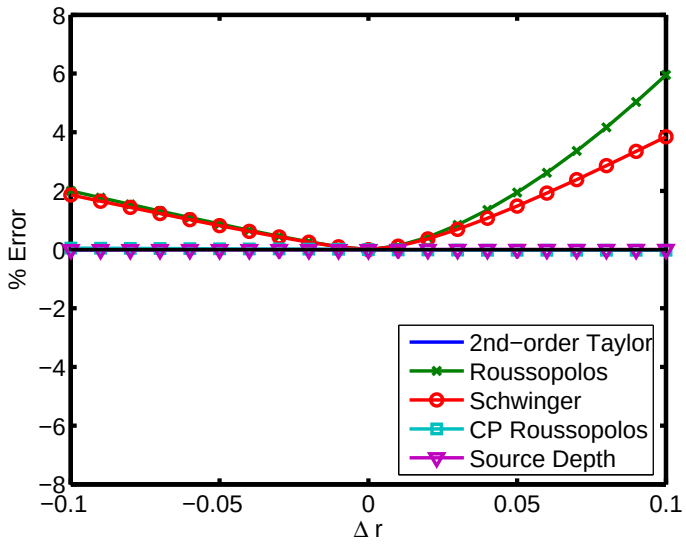

FIG. 5. *Perturbation estimate errors for 8.741 cm Godiva spherical source perturbations with no shielding.*

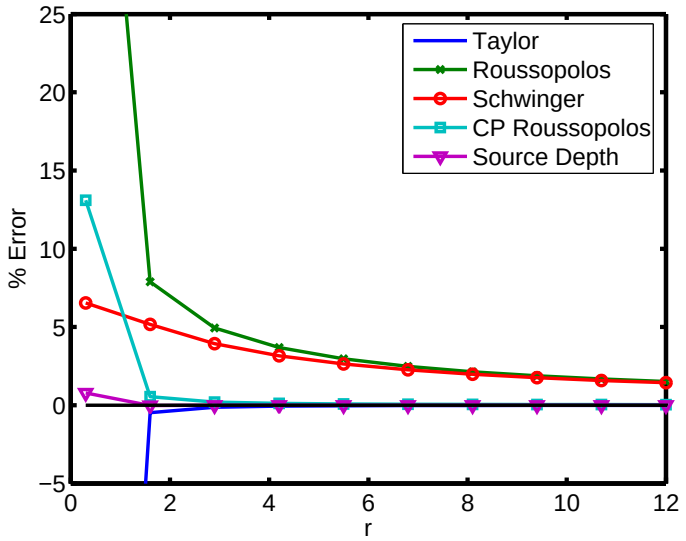

FIG. 6. *Perturbation estimate errors as a function of unperturbed radius for -0.1 cm perturbations of an HEU spherical source with no shielding.*

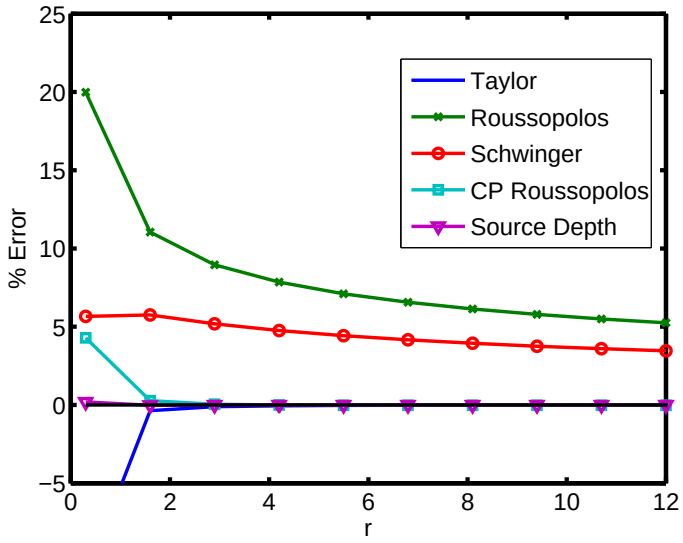

FIG. 7. *Perturbation estimate errors as a function of unperturbed radius for +0.1 cm perturbations of an HEU spherical source with no shielding.*

shield perturbations. To second order,

$$M_C = M_0 - < \psi^* \Delta\Sigma \psi > + \frac{1}{2} \frac{< \psi^* \Delta\Sigma \psi >^2}{M_0} \tag{99}$$

This estimate was used for several shield perturbation problems with a range of perturbation distances, and the convergence rate was extracted using the formula

$$p = \frac{ln(\Delta M_1)/ln(\Delta M_2)}{\Delta r_1 / \Delta r_2} \tag{100}$$

where ΔM_1 and ΔM_2 are the errors in the perturbation estimates for perturbations Δr_1 and Δr_2, respectively, and p is the order of convergence. In all cases, it was found that $p \approx 3$; that is, the error in the estimate (99) appears to be $\mathcal{O}(\epsilon^3)$.

For a monodirectional slab,

$$M' = M_0 e^{\Delta\Sigma_t \Delta r} \tag{101}$$

This gives a poor estimate for the spherical problem. However, for the slab

$$< \psi^* \Delta\Sigma_t \psi > = \Delta\Sigma_t \Delta r M_0. \tag{102}$$

This can be used to rewrite (101) as

$$M_{exp} = M_0 e^{<\psi^* \Delta\Sigma_t \psi> / M_0}. \tag{103}$$

Application of the estimate (103) to the spherical problem gives a very accurate perturbation estimate, as we will see. To second order

$$M_{exp} = M_0 - < \psi^* \Delta\Sigma \psi > + \frac{1}{2} \frac{< \psi^* \Delta\Sigma \psi >^2}{M_0}, \tag{104}$$

explaining the performance of the estimate (99).

Parameter	Value
q_1	38.09993 $\gamma/\text{cm}^3\text{s}$
$\Sigma_{t,1}$	1.91451 cm^{-1}
$\Sigma_{t,3}$	1.00161 cm^{-1}
$\Sigma_{t,4}$	0.187625 cm^{-1}

TABLE 1
Parameters for the spherical perturbation problem

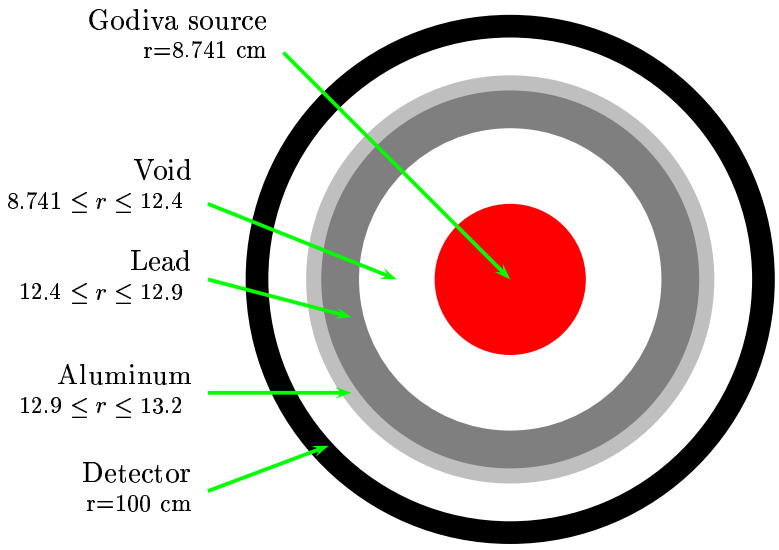

FIG. 8. *Test problem setup*

IV.F Application to a Shielded Spherical Source We now consider the shielded spherical source problem with the same shield interface locations as the shielded slab and source radius $r_1 = 8.741$ cm. The unperturbed configuration is shown in Figure 8. This is the same test problem used in [2, 4, 5], although the macroscopic cross sections differ very slightly. For all perturbation tests, results for the 766-keV line are shown, although some tests were repeated using other lines and similar results were obtained. The volumetric source rate and macroscopic absorption cross sections are given in Table 1.

The Roussopolos coordinate-perturbed (CP) estimate uses the reduced Roussoplos variational functional (72) with the coordinate perturbed adjoint flux (81).

The relative errors in perturbation estimates are plotted in Figure 9 for source perturbations ranging from $\Delta r = -0.1$ to $\Delta r = +0.1$ cm. The Taylor series approximation does very well because the response to source perturbations happens to be nearly linear over this range. Note that the Roussopolos surface formulation of [2] is exactly equivalent to the Taylor approximation.

The Roussopolos variational estimate is much less accurate; the coordinate perturbed Roussopolos

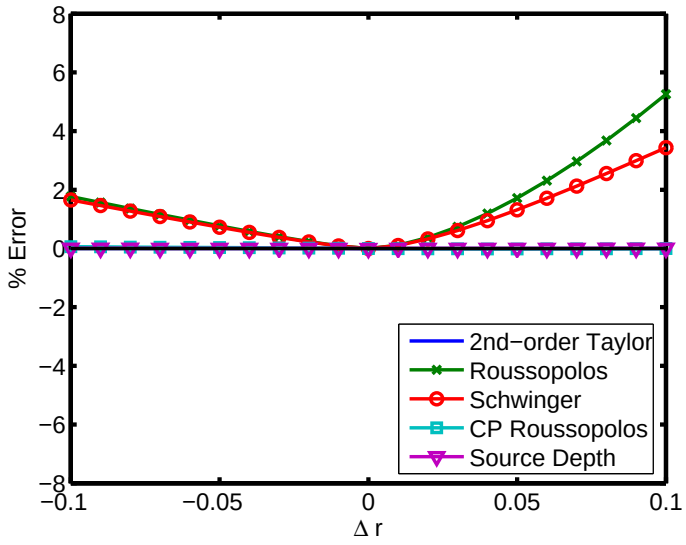

FIG. 9. *Perturbation estimate errors for 8.741 cm Godiva spherical source perturbations with shielding.*

estimate, using

$$\tilde{\psi}^*(r) = \psi^*(r-\epsilon) \quad (105)$$

$$< \tilde{\psi}^*(r,\theta)\tilde{\psi}(r,\theta) > = < \psi^*(r-\epsilon,\theta)\psi(r,\theta) >, \quad (106)$$

is a drastic improvement over the ordinary Roussopolos estimate. In fact, the Taylor, CP Roussopolos, and Source Depth estimates are all very accurate.

In Figure 10, we plot results for the same problem over a more severe range of perturbations. In [2] it was claimed that the Roussopolos surface estimate is highly accurate for this problem because the change in leakage is primarily due to the change in surface area; i.e., $M_d \propto r_1^2$. This assumption is built into the Source Depth estimate, which turns out to be less accurate than the Taylor/Rouss. surf. estimate. On the other hand, the fact that the 1st-order Taylor estimate is highly accurate for outward perturbations indicates that the leakage is approximately a linear function of r_1. The shift from a quadratic to a linear response must be due to the effect of the shielding.

We next consider the spherical problem with source radius 0.3 cm. Perturbations to this source are more difficult to estimate, for two reasons: the source is not saturated, and the surface of the source is far from planar. Results are plotted in Figure 11. Both the Taylor and variational approximations are unable to capture the highly nonlinear sensitivity. The coordinate perturbed Roussopolos approximation does better, and the Source Depth estimate is extremely accurate.

It is illuminating to compare Figure 11 with Figure 4 and Figure 9 with 5. For the 0.3 cm source, the plots with and without shielding look nearly identical. For the 8.741 cm source, the Source Depth estimate is much less accurate in the case of shielding. This implies that the effect of the shielding is essentially linear for the smaller source, but has become nonlinear for the larger source.

We now consider the Godiva source problem and examine perturbations to the shield radii (r_2, r_3, r_4). Figures 12-14 show the errors in perturbation estimates for perturbations to r_2, r_3, r_4, respectively.

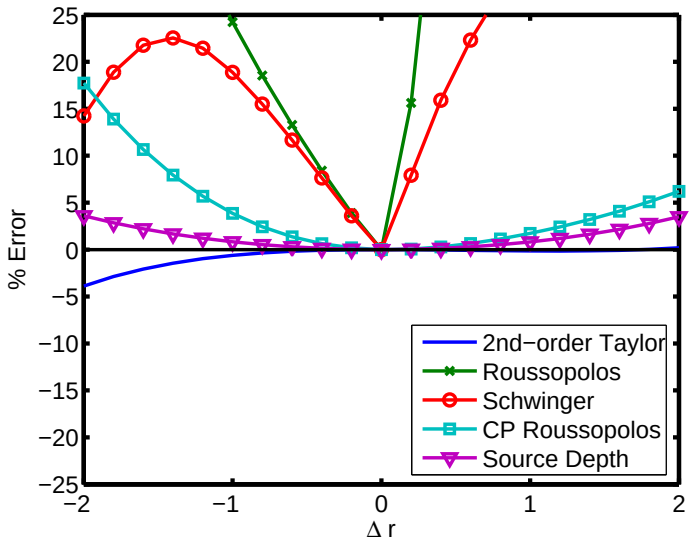

FIG. 10. *Perturbation estimate errors for 8.741 cm Godiva spherical source perturbations with shielding, over a wider range of perturbations.*

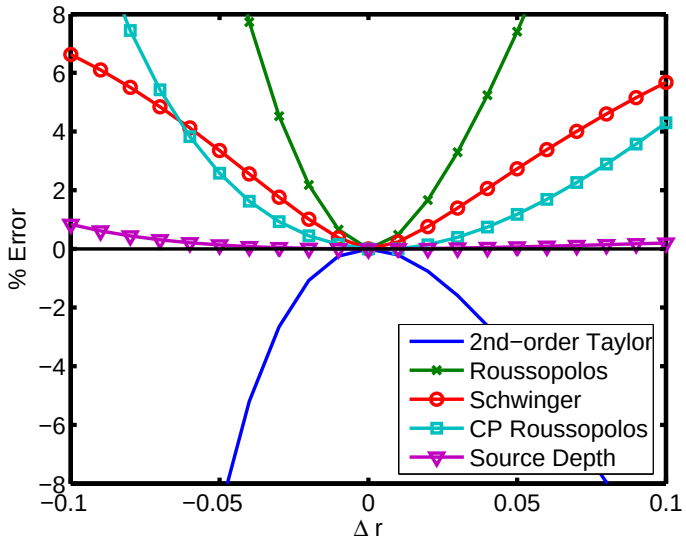

FIG. 11. *Perturbation estimate errors for 0.3 cm spherical source perturbations with shielding.*

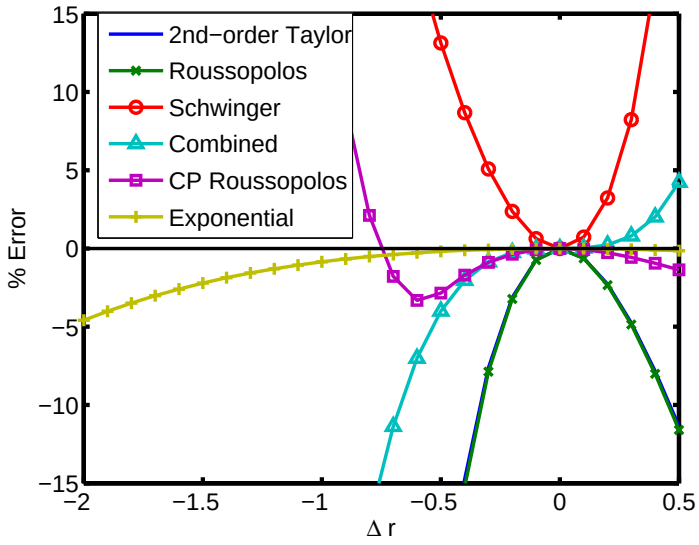

FIG. 12. *Perturbation estimate errors for perturbations to r_2 (8.741 cm source).*

The exponential estimate is clearly superior in every case. Note that the perturbations to r_2 range from a lead shield that is five times as thick to no lead shielding at all, corresponding to leakage perturbations from -90% to $+78\%$. For the case $\Delta r_2 = -2.0$ cm, all the other estimates are in error by more than 200%, but the exponential estimate is accurate to within less than 5%.

Figures 15-17 show results for the same perturbations to the shield radii (r_2, r_3, r_4) with a 0.3 cm HEU source. With this source, the Exponential estimate is accurate to within less than 0.02% for all perturbations.

IV.F.i Multiple Perturbations We now consider problems where both source and shield interfaces are perturbed. Based on the results of the previous section, we would like to combine the Source Depth and Exponential perturbation estimates to obtain a highly accurate estimate for multiple perturbations. The two can be easily combined using the formula

$$M_{MP} = M_{SD} e^{<\psi^* \Delta\Sigma_t \psi>/M_0}. \tag{107}$$

where M_{SD} is given by Eq. (98). That is, the source depth estimate is calculated, ignoring the shield perturbation, and then the result is multiplied by the usual exponential factor for the shield perturbation.

In Table 2, we consider the same set of multiple perturbations that were considered in [4]. The M_{MP} estimate is more accurate than the M_C estimate in all but one case, and in most cases the improvement is by an order of magnitude or more.

V Iterative Inverse Solution Methods

V.A Newton-Raphson Iteration One approach to solving the inverse problem (in the absence of measurement error) is to define an error function $\epsilon(x)$ and use a root-finding method to

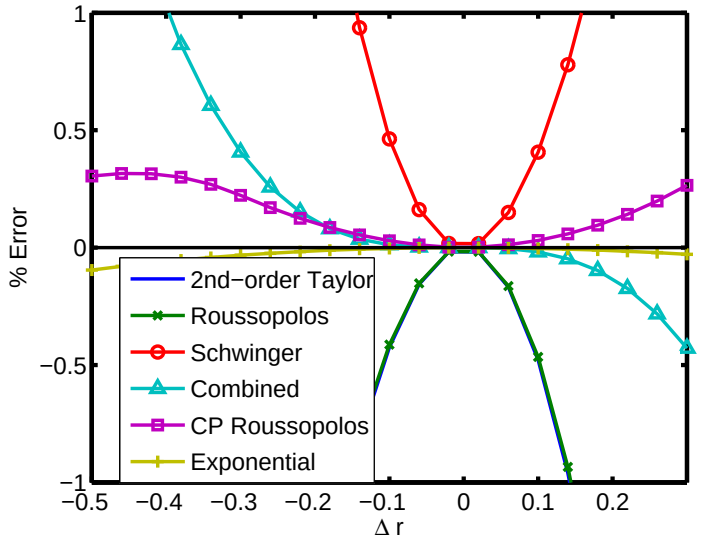

FIG. 13. *Perturbation estimate errors for perturbations to r_3 (8.741 cm source).*

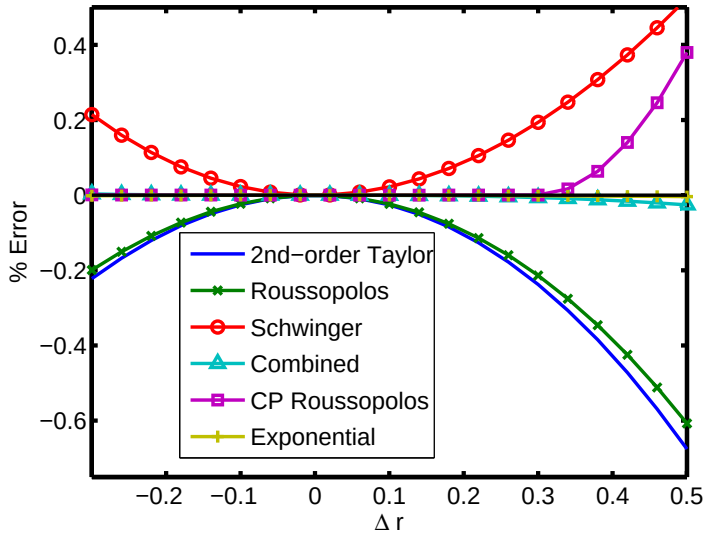

FIG. 14. *Perturbation estimate errors for perturbations to r_4 (8.741 cm source).*

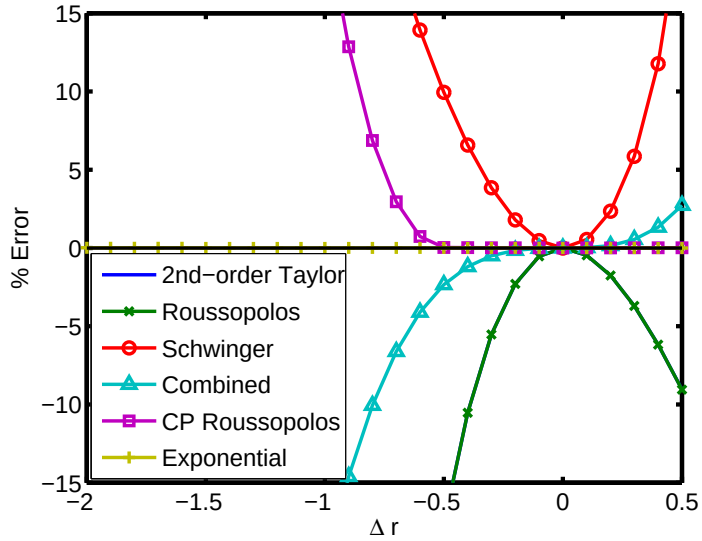

FIG. 15. *Perturbation estimate errors for perturbations to r_2 (0.3 cm source).*

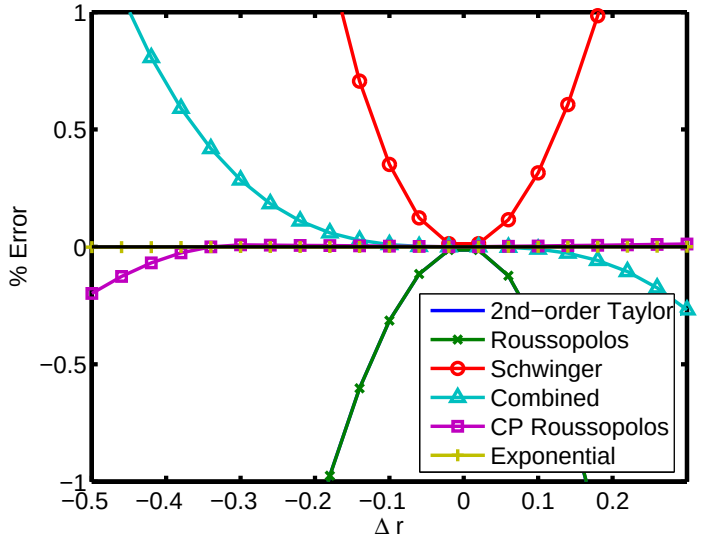

FIG. 16. *Perturbation estimate errors for perturbations to r_3 (0.3 cm source).*

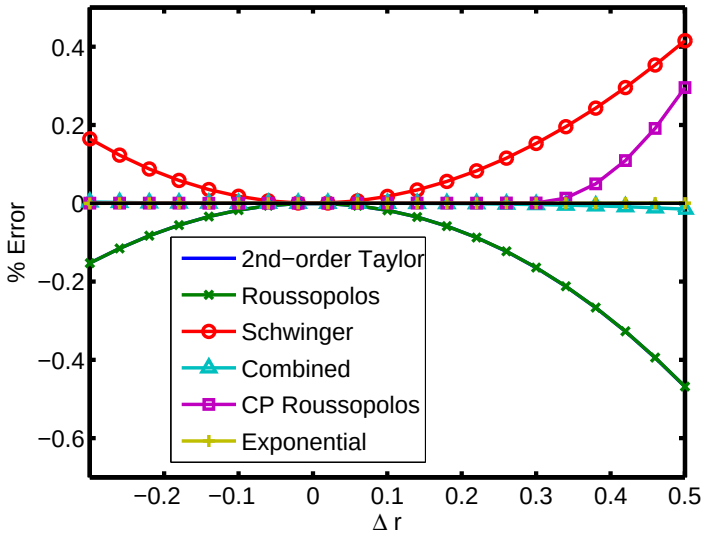

FIG. 17. *Perturbation estimate errors for perturbations to r_4 (0.3 cm source).*

r_1	Δr_1	Δr_3	Exact leakage perturbation (%)	% Error in M_{MP}	% Error in M_C [4]
8.741	-0.2	-0.2	15.56	0.16	1.10
		0	-4.03	0.03	0.22
		+0.2	-20.21	-0.11	-0.83
	+0.2	-0.2	25.68	-0.13	-0.94
		0	4.06	0.03	-0.23
		+0.2	-13.72	0.16	0.54
1.0	-0.1	-0.2	-7.09	-0.04	5.17
		0	-21.06	-0.05	0.73
		+0.2	-32.93	-0.05	-4.25
	+0.1	-0.2	45.34	-0.04	-2.21
		0	23.47	-0.04	0.61
		+0.2	4.89	-0.03	3.87
0.3	-0.1	-0.2	-60.57	0.84	17.58
		0	-66.49	0.84	-4.33
		+0.2	-71.53	0.83	-29.45
	+0.1	-0.2	148.54	0.20	-5.40
		0	111.20	0.20	0.07
		+0.2	79.46	0.20	6.48

TABLE 2

% Errors in the 766-keV line leakage using the combined source depth/exponential estimate for multiple perturbations

solve $\epsilon(x^*) = 0$. A simple error function is the vector of relative errors:

$$\epsilon_i = \frac{M^i(x) - M_0^i}{M_0^i}. \tag{108}$$

In [5], the sum of squared errors was used:

$$\epsilon = \frac{1}{2}\sum_{i=1}^{N}(M^i(x) - M_0^i)^2. \tag{109}$$

Let $\{x_1, x_2, ..., x_N\}^T$ denote the vector of unknowns. Some guess x_0 is provided as a starting point. The Newton-Raphson method is then

$$(\nabla_x \epsilon(x^i))^T \Delta x = -\epsilon(x^i) \tag{110}$$

$$x^{i+1} = x^i + \Delta x, \tag{111}$$

where $\nabla_x \epsilon$ is the gradient of the error function with respect to the unknowns. Note that the gradient is a matrix in the case of (108), while it is a vector in the case of (109). In the former case, the number of observed gamma lines must be greater than or equal to the number of unknowns for Eqn. (110) to have a solution. If the number of gamma lines is greater, Eqn. (110) is solved in the least squares sense. Using the chain rule,

$$(\nabla_x \epsilon)_{jk} = \frac{\partial \epsilon}{\partial M^j}\frac{\partial M^j}{\partial x_k}. \tag{112}$$

A key part of the inverse method is the calculation of the derivatives $\frac{\partial M^j}{\partial x_k}$, which we address in the next two sections. We will see that the variational methods of [2] are equivalent to a Newton-Raphson iteration using error function (108) and adjoint differentiation.

For the error function (108), the Jacobian is

$$\nabla_x \epsilon = \begin{pmatrix} \frac{1}{M_0^1}\frac{\partial M^1}{\partial x_1} & \frac{1}{M_0^1}\frac{\partial M^1}{\partial x_2} & \cdots \\ \frac{1}{M_0^2}\frac{\partial M^2}{\partial x_1} & \ddots & \\ \vdots & & \frac{1}{M_0^G}\frac{\partial M^G}{\partial x_N} \end{pmatrix} \tag{113}$$

$$\nabla_x M = \begin{pmatrix} \frac{\partial M^1}{\partial x_1} & \frac{\partial M^1}{\partial x_2} & \cdots \\ \frac{\partial M^2}{\partial x_1} & \ddots & \\ \vdots & & \frac{\partial M^G}{\partial x_N} \end{pmatrix} \tag{114}$$

Some terms in the derivatives $\frac{\partial M^j}{\partial x_k}$, such as the first term of the RHS of Eqn. (30) depend on q, with q a function of some of the parameters x_i. For these terms, a normalization factor of $\frac{1}{M_d}$ is used in place of $\frac{1}{M_0}$.

In general we expect the Newton-Raphson method to fail for an initial guess sufficiently far from the true solution.

V.B Equivalence of Variational Inverse and Adjoint Differentiation Methods In this section we will show that the inverse methods of [2] are equivalent to Newton-Raphson iteration using the function (108) and adjoint differentiation. We consider specifically the case of unknown radii.

Using (53) and (108),

$$\frac{\partial \epsilon}{\partial r_n} = \frac{4\pi r_n^2}{M_0}\psi^*(r_n)\left(\Delta q - \Delta\Sigma\psi(r_n)\right). \tag{115}$$

Then (110) gives

$$\frac{4\pi r_n^2}{M_0}\psi^*(r_n)\left(\Delta\Sigma\psi(r_n) - \Delta q\right)\Delta r = \frac{M^i(x) - M_0^i}{M_0^i}. \tag{116}$$

On the other hand, the Roussopolos method (Eqn. A.5) of [2] uses the formula

$$\frac{1}{M_0}\left(< \psi^*\Delta\Sigma\psi > - < \psi^*\Delta q >\right) = \frac{M^i(x) - M_0^i}{M_0^i}, \tag{117}$$

with the inner products approximated by (see Eqns. 35a-35b therein)

$$< \psi^*\Delta\Sigma\psi > = \int_{r_n}^{r'_n} \psi^*\Delta\Sigma\psi dV \approx \Delta\Sigma\Delta r \frac{d}{dr}\left(\int_{r_n}^{r'_n} \psi^*\psi dV\right)\Bigg|_{r=r_n} \tag{118}$$

$$< \psi^*\Delta q > = \int_{r_n}^{r'_n} \psi^*\Delta\Sigma\psi dV \approx \Delta q\Delta r \frac{d}{dr}\left(\int_{r_n}^{r'_n} \psi^* dV\right)\Bigg|_{r=r_n}, \tag{119}$$

In [2], the derivatives in these expressions were evaluated via central differences, resulting in the approximations

$$\frac{d}{dr}\left(\int_{r_n}^{r'_n} \psi^*\psi dV\right)\Bigg|_{r=r_n} \approx \frac{1}{2\delta}\int_{r_n-\delta}^{r_n+\delta} \psi^*\psi dV \tag{120}$$

$$\frac{d}{dr}\left(\int_{r_n}^{r'_n} \psi^* dV\right)\Bigg|_{r=r_n} \approx \frac{1}{2\delta}\int_{r_n-\delta}^{r_n+\delta} \psi^* dV, \tag{121}$$

where δ was taken to be the width of six mesh points.

The derivatives in (118-119) can instead be evaluated exactly:

$$\frac{d}{dr}\left(\int_{r_n}^{r'_n} \psi^*\psi dV\right)\Bigg|_{r=r_n} = 4\pi r_n^2\psi^*(r_n)\psi(r_n) \tag{122}$$

$$\frac{d}{dr}\left(\int_{r_n}^{r'_n} \psi^* dV\right)\Bigg|_{r=r_n} = 4\pi r_n^2\psi^*(r_n), \tag{123}$$

Substituting (122-123) in (117) yields (116).

We see that the Roussopolos method of [2] would be equivalent to simple adjoint differentiation if the exact derivatives (118-119) were used. The Schwinger method can be obtained by considering the appropriate normalization of the second term on the right hand side of (53).

A similar analysis considering the derivatives of the leakage with respect to source component weight fraction again shows that the expressions resulting from Roussopolos functional inversion and adjoint differentiation are identical. In this case, inversion of the Schwinger functional yields a different normalization of one term, as noted in [2]. This alternate normalization results in much better performance and is used in all implementations in this paper.

What is the effect of using the approximations (120-121)? The quantities on the right may be considered as approximations either to the derivatives on the left or to the original inner products. In either case, the error in the approximations is $\mathcal{O}(\Delta r^2) + \mathcal{O}(\delta^2)$. In contrast, the approximation error in (118-119) is $\mathcal{O}(\Delta r^2)$. Because δ is a fixed finite value (related to the discrete ordinates mesh), the $\mathcal{O}\delta^2$ error in the gradient will not vanish as x approaches the true solution. The methods of [2] should not be expected to converge to an accuracy smaller than the error produced by this term; one of the test cases in Section VI.B demonstrates this effect.

The Schwinger method was implemented using Eqns. (122- 123); the resulting method is referred to as the Newton-Raphson adjoint method. The use of (122- 123) as approximations to the inner products in (117) is also equivalent to using the surface integral formulation of [4].

V.C Levenberg-Marquardt Optimization When real measurements are involved, root-finding methods like those above may be inappropriate because an exact root may not exist. Instead, one may consider the residual

$$r_i = \frac{M^i - M_0^i}{\sigma^i} \tag{124}$$

where σ^i is the uncertainty in the measurement of M_0^i, and seek to minimize the objective function χ^2:

$$\chi^2 = R(x)^T R(x) = \sum_{i=1}^{G} \left(\frac{M^i - M_0^i}{\sigma^i} \right)^2. \tag{125}$$

Efficient methods for solving this optimization problem require knowledge of the gradient of χ^2:

$$(\nabla_x \chi^2)_j = \frac{\partial \chi^2}{\partial x_j} = \sum_{i=1}^{G} \frac{M^i - M_0^i}{(\sigma^i)^2} \cdot \frac{\partial M^i}{\partial x_j}. \tag{126}$$

Thus the partial derivatives $\frac{\partial M^i}{\partial x_j}$ are again needed.

The Levenberg-Marquardt algorithm iteratively solves

$$x^{i+1} = x^i - ((\lambda + 1) D(R'^T R') + R'(x^i)^T R'(x^i))^{-1} R'(x_i)^T R(x_i) \tag{127}$$

where $'$ denotes differentiation, $D(A)$ is the diagonal part of the matrix A, and λ is a parameter that is adjusted after each iteration. The reader is referred to [6] for full details.

VI Numerical Tests of Inverse Methods

VI.A Numerical Quadrature Some of the integrals derived in the previous sections require special care in order to be evaluated accurately. The integrand of the source radius derivative (Eqn. 23) has a singularity at the upper bound of integration; Matlab's adaptive Simpson quadrature

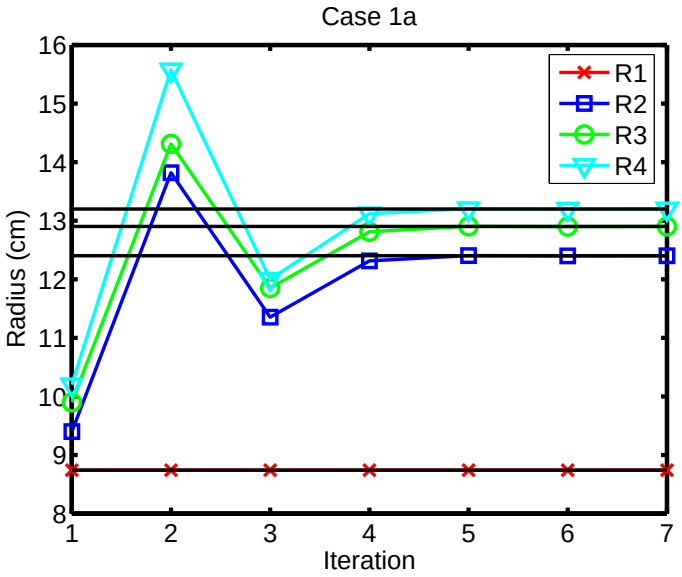

FIG. 18. *Case 1a*

often had difficulty evaluating this integral. The QUADPACK routine, which uses adaptive Gauss-Kronrod quadrature, was able to evaluate this and the other integrals quickly and accurately. QUADPACK is freely available from NETLIB (www.netlib.com).

Because many of the integrands are non-smooth at the angles corresponding to a ray that is tangent to a layer surface, it is sometimes necessary to break the integral up into several integrals, each of which possesses a smooth integrand. Otherwise, some particular region may not be sampled by the quadrature routine and the result will be very inaccurate. For instance, when given a small central source, if the integration bounds are given as $[0, \theta_n]$, where θ_n corresponds to the edge of the largest shield layer, the quadrature software may miss the entire source region and return a zero leakage value. This is not unexpected, because the quadrature software error bounds apply only to smooth integrands.

VI.B Comparison of Root-Finding Methods In this section, we compare results using three root-finding methods. All three use the Newton-Raphson (NR) iteration; they differ only in the calculation of gradients. The first uses the semi-analytic ray-trace gradients; this method is referred to as NR-RT. The second is Favorite's Schwinger method from [2], with averaged values; this method is referred to as NR-SA. The third method is the Schwinger method using point values; this method is referred to as NR-SPV. We use the set of test cases used in [2]. The purpose of this comparison is to show whether the difficulties encountered by the Schwinger method are due to inaccuracies in the derivatives or some other cause.

The unperturbed test problem configuration is shown in Figure 8.

VI.B.i Case 1: Shield Location Unknown In cases 1a and 1b, the initial model had the shield 3 cm too close and 2 cm too far from the source, respectively. The radii calculated at each iteration are plotted in Figures 18 and 19, respectively, for the NR-RT method.

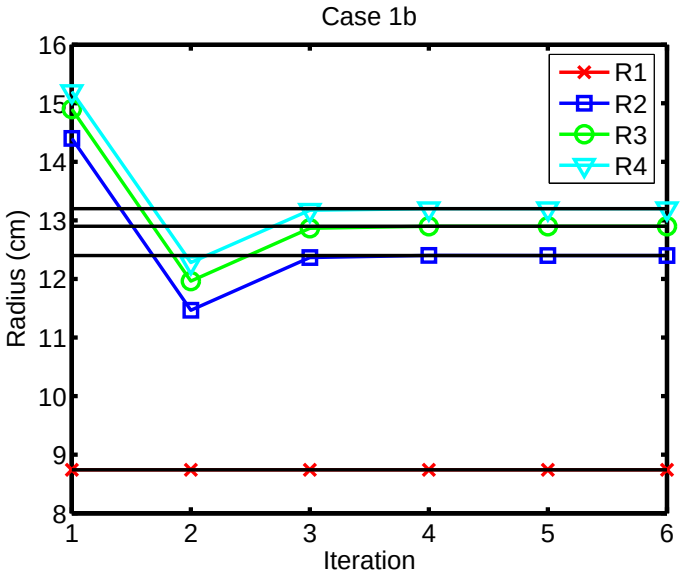

FIG. 19. *Case 1b*

In case 1b, both methods again converge to the correct solution.

In case 1c, the initial model had the shield 2.5 cm too far from the source. NR-SA finds a much thicker aluminum layer after the second iteration and is unable to converge. NR-RT encounters no such difficulty; although the thickness of the Al shield is about 10% too great after the third iteration, the solution converges rapidly. We conclude that the failure of NR-SA in this case is due to inaccuracies in the calculated Jacobian.

NR-SPV converged to the correct solution in a few iterations for all three cases 1a-1c. This suggests that the loss of accuracy due to the averaging procedure used in [2] may be responsible for the non-convergence of NR-SA in case 1c. However, NR-SPV fails in the same manner as NR-SA if the shield is initially moved out 1 cm more.

Each of these cases (1a, 1b, 1c) was solved using the known thickness formulation of Section II.B.ii, allowing only the void layer thickness to vary. Again, NR-RT essentially converged in two iterations, although the result after only 1 iteration was off by no more than a few percent in each case. In general, the known thickness approach is preferable for this problem because it reduces the dimensionality from three to one. In fact, this method is able to converge to the correct solution even when the initial void thickness is increased to about 12 cm. For larger initial thicknesses, the inner shield radius is inside the source radius after the first iteration and the method does not converge.

VI.B.ii Case 2: Shield Thickness and Location Unknown In case 2a, the lead layer was 0.2 cm too thin, the aluminum layer was 2.1 cm too thick, and the shield was 0.1 cm too close to the source. Both NR-SA and NR-RT quickly produce negative values for the shield radii, and thus fail. For case 2b, both methods again fail. In case 2c, NR-RT still fails, while NR-SA converges.

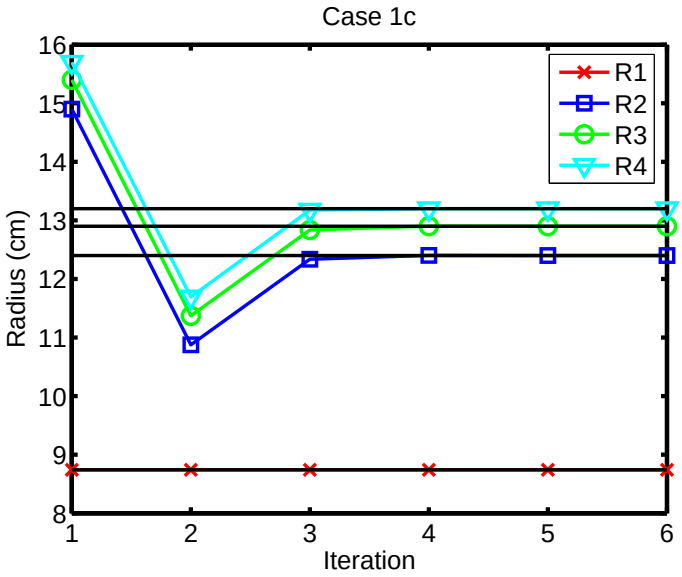

FIG. 20. *Case 1c*

NR-SPV performed similarly to the NR-SA for these cases.

The ill-conditioning of this problem is related to the very weak dependence of the leakage on the shield location. One way to approach this problem is to iterate a few times with the inner shield radius fixed, then allow the inner shield radius to vary. This allows the method to approximately determine the shield thicknesses, and then solve the more difficult problem of shield location. Using this technique, NR-RT was able to converge to the correct solution of case 2a after six iterations of the fixed-location problem plus one iteration of the full problem. Case 2b required 20+3 iterations, and case 2c required 9+1 iterations. The intermediate (fixed-location) solutions were different for case 2a and case 2b, even though the fixed shield location was the same for both.

VI.B.iii Case 3: Source Radius Unknown In cases 3a and 3b, the source radius was 0.5 cm too small and 0.5 cm too large, respectively. In both cases, NR-RT converged in 2 iterations (the error in r_1 was less than 4×10^{-3} after 1 iteration). This shows that the dependence of the leakage on the source radius is nearly linear for perturbations of this magnitude or smaller. In spite of this, NR-SA converges very slowly. This indicates that NR-SA gives a poor approximation to the derivative of the leakage with respect to the source radius.

For case 3a, NR-SPV decreased the source radius in each iteration, indicating that the method was unable even to correctly determine the sign of the derivatives in the Jacobian. For case 3b, it converged in only 8 iterations.

Although the performance of NR-SA appears superior to NR-SPV for source perturbations, in fact the relevant derivative is nearly zero (because the source is near saturation), and the derivatives computed by NR-SPV are uniformly more accurate (despite one of them having the wrong sign).

VI.B.iv Case 4: Source Radius Unknown, Shield Thickness and Location Unknown In case 4, the source radius was 0.159 cm too large, the lead layer was 0.05 cm too thin, the aluminum layer 0.4 cm too thick, and the inner radius of the shield was 0.35 cm too small. NR-SA fails to converge for this problem. NR-RT converges in just a few iterations. The behavior of NR-RT on cases 2 indicates that this convergence may be merely fortuitous in some sense; generally, it may be useful again to roughly solve the problem with the void thickness fixed, then use the result as a starting point for the full problem.

With the threshold for singularity of A raised to 3×10^{-3}, NR-SA converges to a wrong solution. We can examine the behavior of NR-RT to determine why. In fact, using the same increased singularity threshold, NR-RT converges to an incorrect solution. This indicates that the failure of NR-SA is not related to the use of truncated Taylor series in evaluating certain derivatives, as has been suggested. Examining the matrix A corresponding to the exact solution, we find that it has a reciprocal condition number of 1.9×10^{-3}, which is below the singularity threshold. The inverse methods declare the matrix to be singular for all iterations after getting close to the true solution. The inverse methods are unable to find the correct solution because the singularity fix is throwing away significant information about the sensitivities near the exact solution. One way to avoid this is to apply the singularity threshold only when the max-norm of x exceeds some characteristic distance. This will tend to avoid the generation of unphysical radii initially, but will not impede the asymptotic convergence of the method. Such a trigger is desirable because it is conceivable that the same pathology might occur even with the lower singularity threshold. However, this does not cause NR-SA to converge to the correct solution for this problem, because it does not address the difficulty that prevents convergence when the singularity threshold is low.

The source of this difficulty was discovered by running the problem with NR-SPV with the original SVD threshold (2×10^{-5}). In this case, the method converged to the correct solution in 16 iterations. We conclude that NR-SA was unable to locate the exact solution because the approximations (120-121) still give an $\mathcal{O}(\delta^2)$ error as Δr approaches zero when the approximate solution is very near the exact solution.

VI.C Comparison of Optimization Methods In this section, we compare results using two optimization methods. Both use the Levenberg-Marquardt iteration; they differ only in the calculation of gradients. The first uses the semi-analytic ray-trace gradients; this method is referred to as LM-RT. The second uses adjoint differentiation with fluxes calculated using the discrete ordinates code PARTISN, and corresponds to the method of [3]; this method is referred to as LM-ADJ. We again use the set of test cases used in [2].

Table VI.C shows the number of iterations required to converge for each test case; for comparison, the results of the Newton-Raphson methods of the previous section are also included. A blank entry indicates that the method did not converge.

Acknowledgment

This research was performed while on appointment as a U.S. Department of Homeland Security (DHS) Fellow under the DHS Scholarship and Fellowship Program, a program administered by the Oak Ridge Institute for Science and Education (ORISE) for DHS through an interagency agreement with the U.S Department of Energy (DOE). ORISE is managed by Oak Ridge Associated

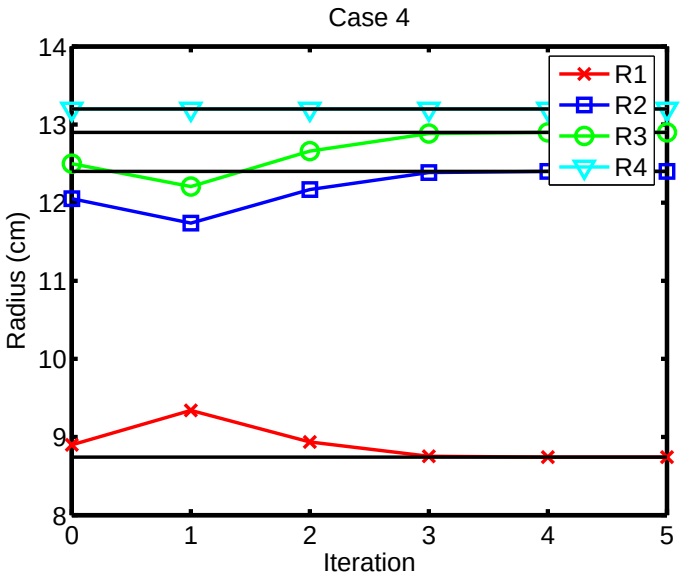

FIG. 21. *Case 4*

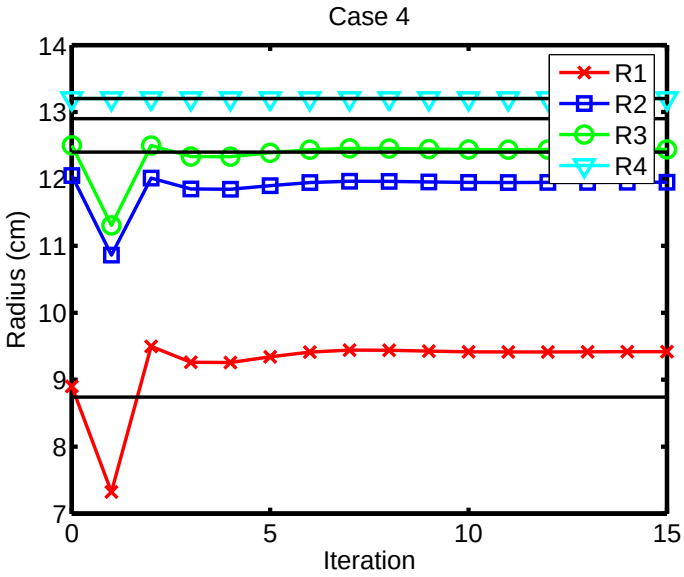

FIG. 22. *Case 4, singularity threshold increased to* 3×10^{-3}.

Unknown	Case	NR-ADJ	NR-RT	LM-ADJ	LM-RT
	1a	4	2*	7	2*
Shield	1b	4	2*	11	2*
Location	1c		2*	11	2*
	1d		2*		2*
Shield	2a		7**	11	9
Location	2b		23**	14	12
& Thickness	2c	7	10**	14	12
Source	3a		2	4	3
Radius	3b	8	2	4	3
Source	4		4		5
& Shield	4a				15
Radii	4b				8

*=Thickness formulation; **=fixed void radius method

TABLE 3

Number of iterations required for each method to converge

Universities under DOE contract number DE-AC05-00OR22750. All opinions expressed in this work are the author's and do not necessarily reflect the policies and views of DHS, DOE, or ORISE.

REFERENCES

[1] Kevin Buescher and Diane E. Vaughan. Gamma-ray transport. Technical report, 2003. unpublished.

[2] Jeffrey A. Favorite. Using the Schwinger variational functional for the solution of inverse transport problems. *Nuclear Science and Engineering*, 146:51–70, 2004.

[3] Jeffrey A. Favorite. Using the Levenberg-Marquardt method for inverse radiation transport problems. Technical report, Los Alamos National Laboratory, 2005. in preparation.

[4] Jeffrey A. Favorite. Variational estimates of internal interface perturbations and a new variational functional for inhomogeneous transport problems. *Nuclear Science and Engineering*, 2005. accepted for publication.

[5] Jeffrey A. Favorite and R. Sanchez. An inverse method for radiation transport. *Radiation Protection Dosimetry*, 2005. accepted for publication.

[6] Donald W. Marquardt. An algorithm for least-squares estimation of nonlinear parameters. *Journal of the Society for Industrial and Applied Mathematics*, 11:431–441, 1963.

[7] Bill Taylor. GRAY ray-tracing mathematics. Technical Report WMT-89-107, Los Alamos National Laboratory, 1990.

DK:DK

Distribution

A. R. Heath, X-5, MS F663, arh@lanl.gov

S. C. Frankle, X-5, MS F663, frankles@lanl.gov

J. S. Sarracino, X-5, MS F663, jxs@lanl.gov

E. Mullen, ADTR-TRO, MS B248, emullen@lanl.gov

J. E. Koster, ADTR-TRO, MS B248, jkoster@lanl.gov

G. E. Reader, ADTR-TRO, MS B248, ger@lanl.gov

J. W. Davidson, CHS, MS K488, wdavidson@lanl.gov

M. A. Yates, CHS, MS K488, may@lanl.gov

M. G. Sheppard, X-4, MS T086, sheppard@lanl.gov

J. B. Beck, X-4, MS T087, beckj@lanl.gov

M. W. Kirkland, X-4, MS T086, mkirkland@lanl.gov

K. C. Bledsoe, X-5, MS F663, kbledsoe@lanl.gov

R. C. Little, X-5, MS F663, rcl@lanl.gov

T. K. Moeller, X-5, MS F663, tmoeller@lanl.gov

R. R. Roberts, X-5, MS F663, rrr2@lanl.gov

J. A. Favorite, X-5, MS F663, fave@lanl.gov

X-DO File

X-5 File